Field enhancement in a circular aperture surrounded by a single channel groove

Nicolas Bonod, Evgeny Popov, Davy Gérard, Jérome Wenger, and Hervé Rigneault

Institut Fresnel, Unité mixte de recherche de CNRS 6133, Aix-Marseille Université, case 161, ave. Escadrille Normandie-Niemen, 13397 Marseille, Cedex 20, France
Corresponding author: nicolas.bonod@fresnel.fr

Abstract: Numerical analysis of diffraction by a single aperture surrounded by a circular shallow channel in a metallic screen shows the possibility of a 50-fold increase of the electric field intensity inside the central aperture, when compared to the incident field. Detailed analysis of cavity modes and their coupling through surface plasmon wave determine the parameters leading to maximum field enhancement. This effect can be used in high-efficiency single-molecule fluorescence analysis in attoliter volumes.

OCIS codes: (240.6680) Surface plasmons; (180.2520) Fluorescence microscopy; (050.1220) Apertures; (140.3945) Microcavities; (310.6628) Subwavelength structures, nanostructures

References and links

1. E. A. Ash and G. Nicholls, "Super-resolution aperture scanning microscope," Nature **237**, 510-511 (1972).
2. A. Lewis, M. Isaacson, A. Harootunian, and A. Muray, "Development of a 500 Å spatial resolution light microscope I. Light is efficiently transmitted through λ/16 diameter apertures," Ultramicroscopy **13**, 227-232 (1984).
3. E. Betzig, A. Lewis, A. Harootunian, M. Isaacson, and E. Kratschmer, "Near-field scanning optical microscopy (NSOM), development and biophysical applications," J. Biophys. **49**, 269-279 (1986).
4. H. A. Bethe, "Theory of diffraction by small holes," Phys. Rev. **66**, 163-182 (1944).
5. J. D. Jackson, *Classical Electrodynamics*, 3rd ed., (John Wiley, New York, 1998).
6. T. W. Ebbesen, H. J. Lezec, H. F. Ghaemi, T. Thio, and P. A. Wolff, "Extraordinary optical transmission through subwavelength hole arrays," Nature **391**, 667-669 (1998).
7. E. Popov, M. Nevière, S. Enoch, and R. Reinisch, "Theory of light transmission through subwavelength periodic hole arrays," Phys. Rev. B **62**, 16100-16108 (2000).
8. S. Enoch, E. Popov, M. Nevière, and R. Reinisch, "Enhanced light transmission by hole arrays," J. Opt. A: Pure and Applied Optics **4**, S83-S87 (2002)
9. M. J. Levene, J. Kotach, S. Turner, M. Foquet, H. G. Craighead, and W. W. Webb, "Zero-mode waveguide for single-molecule analysis at high concentrations," Science **209**, 682-686 (2003).
10. H. Rigneault, J. Capoulade, J. Dintinger, J. Wenger, N. Bonod, E. Popov, T. Ebbesen, and P. F. Lenne, "Detection enhancement of single molecules at high concentrations in subwavelength apertures," Phys. Rev. Lett. **95**, 117401 (2005).
11. E. Popov, M. Nevière, J. Wenger, P.-F. Lenne , H. Rigneault, P. Chaumet, N. Bonod, J. Dintinger, and T. Ebbesen, "Field enhancement in single subwavelength apertures," J. Opt. Soc. Am. A **23**, 2342-2348 (2006).
12. E. Popov, M. Nevière, A.-L. Fehrembach, and N. Bonod, "Optimization of plasmon excitation at structured apertures," Appl. Opt. **44**, 6141-6154 (2005).
13. N. Bonod, E. Popov, and M. Neviere, "Differential theory of diffraction by finite cylindrical objects," J. Opt. Soc. Am. A **22**, 481-490 (2005).
14. F. J. Garcia-Vidal, L. Martin-Moreno, and J. B. Pendry, "Surfaces with holes in them: new plasmonic metamaterials," J. Opt. A: Pure Appl. Opt. **7**, S97-S101 (2005).
15. E. Popov, N. Bonod, and S. Enoch, "Comparison of plasmon surface wave on shallow and deep 1D and 2D gratings," Opt. Express **15**, 4224-4237 (2007).
16. M. Nevière, The Homogeneous Problem in *Electromagnetic Theory of Gratings*, R. Petit, ed., (Springer, 1980) Chap. 5.
17. F. I. Baida, "Enhanced transmission through subwavelength metallic coaxial apertures by excitation of the TEM mode," Appl. Phys. B **89,** 145-149 (2007).
18. A. Snyder and J. Love, *Optical Waveguide Theory* (Kluwert Academic, Boston, 1983).
19. F. Baida, A. Belkhir, and D. Van Labeke, "Subwavelength metallic coaxial waveguides in the optical range: Role of the plasmonic modes," Phys. Rev. B **74**, 205419 (2006).

#90072 - $15.00 USD Received 26 Nov 2007; revised 15 Jan 2008; accepted 15 Jan 2008; published 1 Feb 2008

1. Introduction

Light transmission through single or periodically arranged apertures has attracted the interest of scientists, at first, due to the possibility to confine the electromagnetic field into a relatively small region, smaller than the diffraction limit in free space, thus generating evanescent wavevectors, leading to increased resolution in optical microscopy [1-3]. Even the early studies have shown [2] that the transmission values exceed significantly scalar theoretical predictions [4, 5]. The observation made by Ebbesen, *et al.*, [6] that in periodically arranged array of apertures the transmission enhancement can be almost 100 times stronger, was sufficient to attract the special attention of scientific community. Although the role of the surface plasmon excitation by the periodicity of the geometry was already invoked in this work, it generated many theoretical and numerical studies aiming to explain this phenomenon. While the first attempts were made by use of models with one-dimensional (1-D) periodicity (classical lamellar gratings), it was necessary to apply a two-dimensional periodicity analysis to better understand the complexity of the process. In a few words, while the periodical arrangement of the apertures is responsible for the surface plasmon excitation on both sides of the metallic sheet, the tunnelling of the field inside the apertures is made through the fundamental waveguide mode supported by the hollow metallic waveguide inside the holes [7, 8]. While 1-D slits can support the TEM mode which has no cut-off, this mode cannot propagate in 2-D apertures (coaxial apertures being the exception), and even the fundamental mode has a cut-off and thus the optical field is evanescent inside small apertures. A new application was born [9, 10] that profits from the small size of the cross-section area of single apertures, combined with the exponential decrease of the electromagnetic field inside it gives the possibility to significantly reduce the investigated volume (down to a few attoliters) for single-molecule probing in solutions with micromolar concentrations. In addition, and quite helpfully, when the fundamental mode is close to its cut-off, there is a substantial (6-7 fold) increase of the local field intensity inside the aperture [10, 11] that contributes to enhance the detected signal. This can be explained by the fact that close to the cut-off the mode group velocity tends to zero, so that its field is "accumulated" at the aperture opening.

As already mentioned for hole arrays, the periodicity of the structure can lead to significant local field enhancement by resonantly exciting surface plasmons. A single aperture can have the surrounding metal surface structured in a specific manner in order to better excite the surface plasmon. Instead of the simple periodicity, the structuring has to follow rules established in cylindrical geometry, where Bessel functions naturally substitute the exponentials that serve as basic functions in Cartesian coordinates [12]. The first problem is that one ends up with relatively complex structures of quasi-periodic concentric grooves which are difficult to reliably fabricate and control.

The second problem is that from the point of view of practical applications, only the final excitation intensity per surface unit matters. With the aperture surrounded by concentric grooves, it is necessary that both the surface structure and the incident wave cover a diameter of about 4 times the wavelength. This limits the focusing of incident light and the incoming intensity per surface unit (for a fixed input power). Therefore, even with large enhancements, the excitation intensity in the central aperture may not be significantly higher than the intensity reached with a tightly focused laser beam without the nanostructure. For instance, in the case of a bull's eye structure, the relative electromagnetic enhancement is about 100 (computed for an incoming plane wave), but the structure radius and thus the laser beam focus spot are about 4 times the diffraction limit (minimum focus size). If we compare the net intensity reinforcement to the case of a diffraction-limited spot, the intensity reached with the bull's eye is increased by $100 \times (1/4)^2 = 6.25$, which is about the reinforcement reached with a single (bare) aperture. Still, more complex nanostructures can further improve practical realizations by increasing the emission rate of molecules or modifying the emission radiation pattern to improve the detection efficiency.

The aim of this paper is to study the possibility of field enhancement by using the combined effect of simultaneous excitation of cavity resonances inside the aperture and in a

#90072 - $15.00 USD Received 26 Nov 2007; revised 15 Jan 2008; accepted 15 Jan 2008; published 1 Feb 2008

surrounding channel groove, situated on the illuminated side of the metal layer, these resonances coupled through the surface plasmon wave. This triple interaction results in 30-50 fold field enhancement in the opening of the central aperture. To this aim, it is sufficient to use a single channel of about one wavelength diameter, i.e., enabling strong focusing of the incident beam down to the diffraction limit. Therefore, the net excitation intensity reinforcement in the central aperture is 30-50 fold as compared to the maximum intensity reached in a diffraction limited focused spot. Moreover, a single channel is much simpler to fabricate than a large-area quasiperiodic channels.

For the sake of completeness, we review in Sec. 2 the waveguide mode excitation in a single aperture and its effect on the field enhancement. The modes in the coaxial channel are described in Sec. 3, and their effect on the field in the central region is described in Sec. 4, together with a theoretical and numerical analysis of the role played by the surface plasmon that can propagate along the metal-glass surface.

Numerical analysis is made using the differential method formulated in cylindrical coordinates using Fourier-Bessel functions basis [13] and using eigenvalue/eigenvector technique due to the piecewise invariance of the geometry along the z-axis.

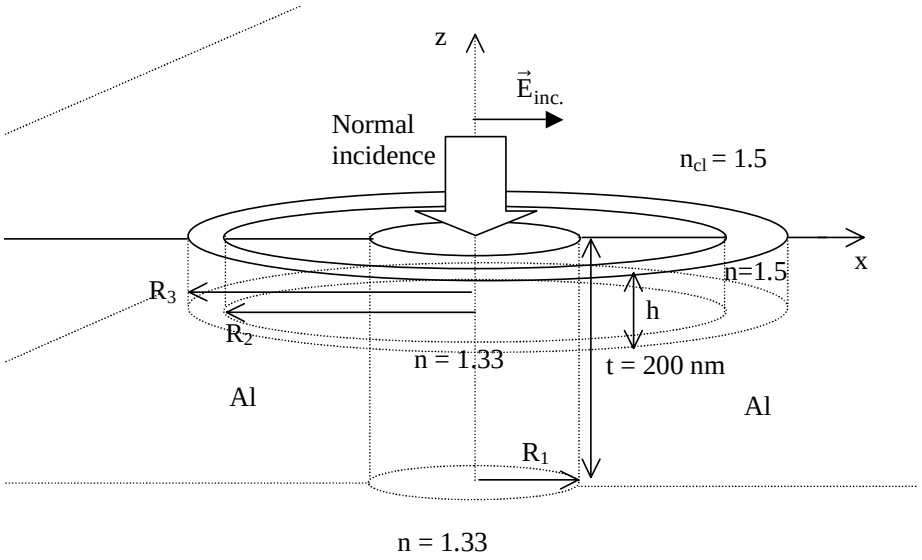

Fig. 1. Schematic representation of a screen with a circular aperture and a circular channel around it, made in an aluminum screen with thickness t = 200 nm. The cladding is glass and the substrate is water. The channel width is $R_3 - R_2$, its depth h, and it is filled with glass.

2. Intensity enhancement – effect of the channel

The structure under study is presented schematically in Fig. 1. It represents a 200 nm thick aluminum screen with a circular aperture filled with water, as is the substrate, as well. The cladding is glass, which fills also a surrounding circular channel with depth h. The structure is illuminated by a plane wave incoming from the glass side, with wavelength λ = 488 nm and linear polarization along the x-axis. We chose that configuration in order to have the maximum intensity enhancement in epi-configuration (illumination and detection from the glass side), with the metal structure restricting the observation volume to the inner of the aperture. This corresponds to the configuration leading to the best results in single molecule fluorescence analysis [10], which determines the choice of water as a substrate. The complex refractive index of aluminum at 488 nm is equal to 0.628 + i 5.452.

Throughout this paper, we will consider the averaged intensity I_S over the central aperture in a plane located at the entrance (z = 0) of the aperture:

#90072 - $15.00 USD Received 26 Nov 2007; revised 15 Jan 2008; accepted 15 Jan 2008; published 1 Feb 2008

$$I_S = \frac{1}{\pi R^2} \int_S \left|\vec{E}\right|^2 dS \quad (1)$$

normalized in a such way that the incident electric field amplitude is equal to unity. For a single circular aperture, a sharp maximum is observed [10, 11] when $R \approx 75$ nm , a value lying below the cut-off dimensions for the fundamental waveguide mode supported inside the hollow metallic waveguide formed inside the aperture.

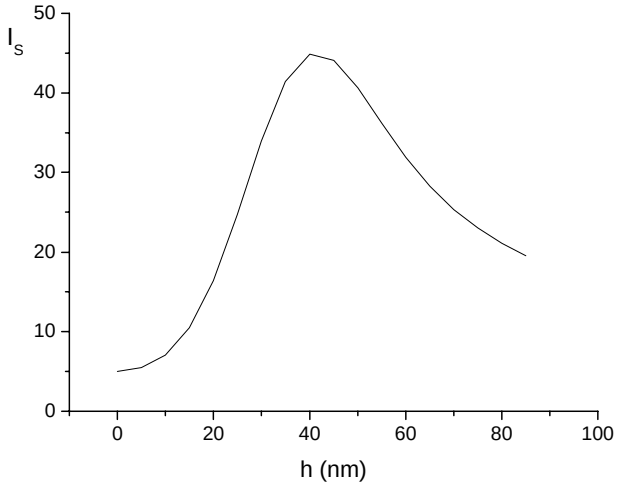

Fig. 2. Field enhancement averaged in the entrance plane of the aperture as a function of the channel depth h for $R_1 = 75$ nm, $R_2 = 200$ nm, $R_3 = 280$ nm.

The introduction of a channel around the aperture can multiply I_S by a factor of 6-9, as observed in Fig. 2, which presents the influence of the channel depth h on the field intensity inside the axial aperture, for $R_2 = 200$ nm and $R_3 = 280$ nm. R_1, R_2 and R_3 values were chosen to obtain the maximum effect. The dependence of the enhancement factor on R_2 for three different values of the channel width $R_3 - R_2$ are presented in Fig. 3 and one observes a well-defined maximum around $R_2 = 200$ nm, a value explained in Sec. 4.1. In order to keep the investigated volume small, the depth of the channel has to be kept relatively small compared to the screen thickness, otherwise it is possible to enhance the transmission by tunneling through the channel bottom. When h = 0 (i.e. no channel), the enhancement is about 6-fold as compared to free space, while the channel can enhance it substantially. The large enhancement brought by the channel groove can seem strange, taking into account that there is no possibility that the excitation of the coaxial cavity resonances could directly influence the field in the central aperture by tunneling through the metal walls, 125 nm thick in our case. Such coupling can happen only through the surface plasmon wave, propagating along the interface metal-glass, as discussed in Sec. 4. The small depth of the channel leading to maximum field enhancement can be understood in analogy with the 1-D periodical diffraction gratings, where the deeper channels modify substantially the plasmon propagation constant and increase its losses [14, 15]. The optimal excitation of surface plasmon waves along metallic gratings happens when the groove depth is about 10% of the wavelength [16], a value observed also for circular channel in Fig. 2.

Given the optimal channel depth, the dependence of the enhancement factor on R_2 and R_3 is presented in Fig. 3 and Fig. 4. The optimal value of 200 nm for the radius R_2 of the inner channel wall is discussed in Sec. 4, and is due to the optimal coupling between the incident

#90072 - $15.00 USD Received 26 Nov 2007; revised 15 Jan 2008; accepted 15 Jan 2008; published 1 Feb 2008

wave and the plasmon surface wave, at one side, and between the coaxial modes and the plasmon, at the other.

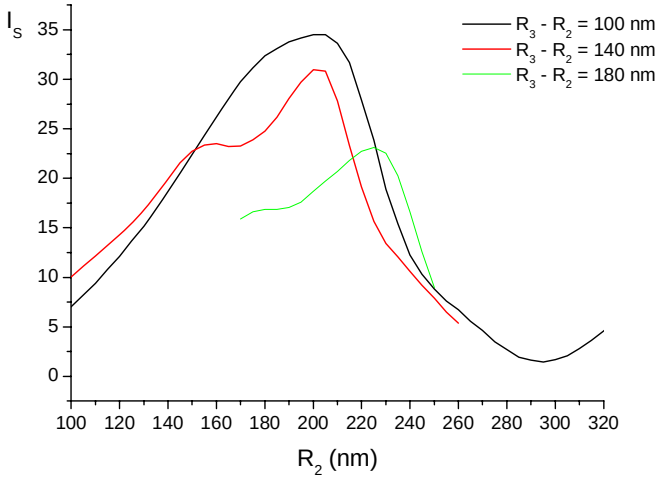

Fig. 3. Enhancement factor as a function of the radius R_2 of the inner channel wall for three different channel widths taken for R_1 = 75 nm and h = 40 nm.

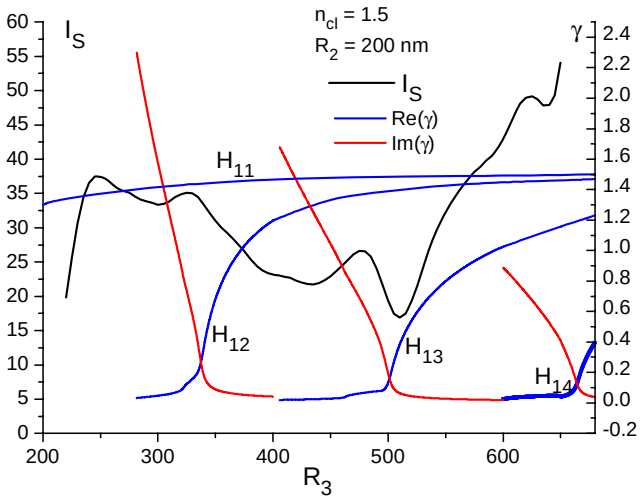

Fig. 4. Enhancement factor I_S (on the left) and the real and imaginary parts of the normalized mode propagation constants γ inside the coaxial channel (on the right) as a function of R_3. R_1 = 75 nm, R_2 = 200 nm, n_{cl} = 1.5 and h = 40 nm.

3. Cavity resonances inside the channel

When the outer radius R_3 of the channel increases, one observes several maxima and minima in Fig. 4. To understand this behavior, we also present on Fig. 4 the propagation constants of the modes inside the channel, defined later in Eq. (2). The determination of the propagation constants is rather straightforward for circular waveguide with perfectly conducting walls, coaxial or not. Introducing cylindrical coordinates (ρ, φ, z) with z-axis lying along the aperture axis, the elementary solutions in Fourier-Bessel basis are the solutions with φ-

#90072 - $15.00 USD Received 26 Nov 2007; revised 15 Jan 2008; accepted 15 Jan 2008; published 1 Feb 2008

dependence following that of the incident field, which is represented for normal incidence and x-polarization in the last column of Table 1, with the notations defined in Eqs. (2) and (3).

Table 1. Radial and azimuthal dependence of the electric field for H- and E-mode, and incident wave. The coefficients a_E and a_H are constants.

	H mode	E mode	E incident	φ-dependence
	$\frac{J_1(k_\rho\rho)+a_H Y_1(k_\rho\rho)}{k_\rho\rho}$	$J_1'(k_\rho\rho)+a_E Y_1'(k_\rho\rho)$	1	$\cos\varphi$
	$J_1'(k_\rho\rho)+a_H Y_1'(k_\rho\rho)$	$\frac{J_1(k_\rho\rho)+a_E Y_1(k_\rho\rho)}{k_\rho\rho}$	1	$-\sin\varphi$
	0	$\frac{J_1(k_\rho\rho)+a_E Y_1(k_\rho\rho)}{ik_z\rho}$	0	$\cos\varphi$

Coaxial channel can have electromagnetic cavity resonances, which represent the mode guided by the corresponding infinitely long coaxial waveguide. It can support a TEM mode that has no cut-off, a property that could enhance the transmission through coaxially structured small apertures [17]. However, in normal incidence this mode cannot be excited with linearly polarized light, because of the different symmetry of the electromagnetic fields of the linearly polarized wave and the TEM mode, the latter having only radial ρ-component of the electric field, which is invariant in φ. The other modes are of two types [18], H (or TE, for transverse electric) modes with zero axial electric field component, and E (or TM, transverse magnetic) modes with zero axial magnetic field component. The ρ-dependence of these modes (having the same φ-dependence of the electric field as the incident field), are listed in Table 1, together with the components of the incident electric field. The z-dependence is given by

$$\exp(ik_z z) \equiv \exp(ik_0\gamma z) \tag{2}$$

with a normalized propagation constant γ in z-direction , and

$$k_\rho^2 + k_z^2 = k^2 = k_0^2 n^2 \tag{3}$$

Here k is the wavenumber inside the waveguide, k_0 is the free-space wavenumber and n is the refractive index of the channel filling medium.

In the case of a single aperture containing the axis, the coefficients $a_{E,H}$ are put equal to zero, because the Bessel functions Y_1 diverge in origin. The same is valid for the plasmon surface wave that can be excited along the surface of the metallic layer, and its field dependence is the same as for the E-modes:

$$\begin{aligned}
E_\rho &= J_1'(k_{\rho,pl}\rho)\cos\varphi \equiv \frac{1}{2}\left[J_0(k_{\rho,pl}\rho) - J_2(k_{\rho,pl}\rho)\right]\cos\varphi \\
E_\varphi &= -\frac{J_1(k_{\rho,pl}\rho)}{k_{\rho,pl}\rho}\sin\varphi \equiv -\frac{1}{2}\left[J_0(k_{\rho,pl}\rho) + J_2(k_{\rho,pl}\rho)\right]\sin\varphi \\
E_z &= \frac{J_1(k_{\rho,pl}\rho)}{ik_{z,pl}\rho}\cos\varphi \equiv \frac{k_{\rho,pl}}{2ik_{z,pl}}\left[J_0(k_{\rho,pl}\rho) + J_2(k_{\rho,pl}\rho)\right]\cos\varphi
\end{aligned} \tag{4}$$

In the case of highly conducting layer material, the plasmon surface wave has a propagation constant in ρ-direction only slightly exceeding the wavenumber in the cladding,

#90072 - $15.00 USD Received 26 Nov 2007; revised 15 Jan 2008; accepted 15 Jan 2008; published 1 Feb 2008

$k_{\rho,pl} > k_0 n_{cl}$ and its magnetic field vector is almost parallel to the surface (corresponding to TM polarization in Cartesian coordinates), thus the field is close to the field of the E-mode close to its cut-off.

The coaxial modes are determined to fulfill the boundary conditions at the vertical walls, where E_φ and E_z have to vanish:

$$\begin{aligned} J_1'(k_\rho R_2) + a_H Y_1'(k_\rho R_2) &= 0 \\ J_1'(k_\rho R_3) + a_H Y_1'(k_\rho R_3) &= 0 \end{aligned}, \quad \text{H mode} \tag{5}$$

$$\begin{aligned} J_1(k_\rho R_2) + a_E Y_1(k_\rho R_2) &= 0 \\ J_1(k_\rho R_3) + a_E Y_1(k_\rho R_3) &= 0 \end{aligned}, \quad \text{E mode} \tag{6}$$

The cut-off appears when $\gamma = 0$, i.e. $k_\rho = nk_0$, so that for the central aperture, the first root of Eq. (5) is $R \approx 108$ nm, when λ = 488 nm and n = 1.33. The smallest cut-off radius of the E-mode is almost twice that of the H-mode and is of less interest for field localization in small volumes. Finitely conducting walls allow for the field penetration inside them and thus the cut-off radius is reduced. For the case of aluminum, the cut-off radius of the central aperture becomes R_1 = 85 nm, and the maximum value of I_S is reached slightly below this cut-off, thus the choice of R_1 = 75 nm.

In coaxial waveguides, the mode propagation constants of the H and E modes are rather different when the inner diameter is smaller compared to the wavelength. The fundamental H_{11} mode has a large cut-off wavelength, given approximately by the relation [19] $\lambda_c \approx \pi(R_2 + R_3)n$, and thus the cut-off radius is quite small, in the case of λ = 488 nm and n = 1.5. For R_2 = 200 nm, the exact [numerically determined from Eq. (5)] cut-off value of R_3 is equal to 55 nm, smaller than R_1. Thus, this mode is always propagating in our conditions.

Higher modes behave in a completely different manner. For mode H_{1m} and a perfectly conducting metal, the cut-off wavelength λ_c is determined by the width of the channel, $\lambda_c \approx 2n(R_3 - R_2)/(m-1)$. In addition, the difference between the E and the H modes diminishes with the growth of the inner diameter, and becomes almost negligible, when $R_2 \approx \lambda/n$, as can be observed in Table 2 for n = 1.5. As can be observed, already at R_2= 200 nm, we are quite close to the limit value of the cut-off width, equal to λ/2n, and shown in the last column of Table 2.

Table 2. The cut-off width $R_3 - R_2$ (in nm) for the modes H_{12} and E_{11} of a coaxial waveguide with infinitely conducting walls at λ = 488 nm and n = 1.5, given for different values of R_2.

R_2	50	100	200	∞
H mode	175	168	164	162.7
E mode	207	180	167	162.7

The cut-off position in the case of finite conductivity is not well-defined as for perfect conductivity, because there is a gradual transfer from evanescent (small radii) to propagating (larger radii) character, as can be clearly observed in Fig. 4, where the dependence of the real and imaginary parts of γ of the cavity resonances inside the coaxial channel are plotted as a function of R_3.

In the case of aluminum, the first mode cut-off can be approximately defined at $R_3 - R_2$ = 135 nm (compared with 164 nm for perfect conductivity) using the data in Fig. 4, the value of R_3 taken where the imaginary part of the γ almost vanish. However, one observes the position of maximum field enhancement at lower radii. In addition, the excitation of the second cavity resonance is accompanied by a minimum of I_S, contrary to the excitation of the first and the

#90072 - $15.00 USD Received 26 Nov 2007; revised 15 Jan 2008; accepted 15 Jan 2008; published 1 Feb 2008

third modes (Fig. 4). There are several factors that complicate the simple link between the cavity resonances in the channel and the field enhancement inside the central aperture.

First, as already discussed, the surface plasmon that propagates along the aluminum/ cladding interface is the only channel of coupling between the cavity modes in the central aperture and in the circular channel. However, the interaction between the plasmon surface wave and the cavity modes will modify both of them [14]. Thus the exact role of the cavity resonances has to be determined by taking into account the finite depth of the channel, which is made numerically in the calculations of I_S, but cannot be evaluated analytically.

Second, the maximum field enhancement can be expected not at the mode cut-off radius, but below it, at radii corresponding to the minimum of the real part of γ, where the group velocity of the cavity resonance in z-direction is null, because this will correspond to accumulation of energy at the channel opening. This can explain why local maxima of I_S can be observed below the cavity mode cuts [Fig. (4)]. However, due to the small channel depth, neither the cuts nor their role in the field enhancement in the central aperture can be determined without taking into account the next point.

Third, the interaction between the plasmon surface wave and the cavity modes is determined by the coupling integral of their fields, which depends strongly on R_2 and R_3, as discussed in the next section.

Fourth, the plasmon surface wave exhibits its own resonances due to the scattering on the channel walls, which will have their influence on the field in the central region.

The last two factors are discussed in detail in the next section.

4. Role of plasmon surface wave

4.1. The choice of the channel inner wall

In the approximation of infinitely conducting walls, the cavity modes have vanishing φ- and z-electric field components at R_2 and R_3, thus the coupling between the surface plasmon and the coaxial cavity modes will be maximal when the plasmon field $\vec{E}_{pl}$ will satisfy the same conditions. From Table 1 it is evident that the condition is equivalent to a zero of the azimutal and axial components. Figure 5 presents the dependence of

$$\mathrm{abs}[J_0(k_{\rho,pl}R_2)+J_2(k_{\rho,pl}R_2)] \tag{7}$$

on R_2 (red curve), compared with the same dependence of the enhancement factor I_S, when $R_3 - R_2 = 100$ nm with $k_{\rho,pl} = k_0\ (1.5578 + i\ 0.01425)$. As it can be observed, the zero of Eq. (7) is located around 185 nm, a value smaller than 200 nm corresponding to the maximum of I_S. This difference can be easily understood taking into account that for finitely conducting walls, the electric field penetrates inside them at 10-15 nm, so that the zeros of Eq. (7) must appear at values smaller than R_2.

Another factor that plays an important role for the field excitation is the direct coupling between the incident wave and the plasmon surface wave due to the scattering on the channel walls. The coupling integral when $\rho = R_2$ is given as:

$$\frac{1}{2\pi}\int_0^{2\pi} \rho\, d\varphi\, \vec{E}_{pl}.\vec{\bar{E}}_{inc} = R_2 J_0(k_{\rho,pl}R_2) \tag{8}$$

where the overbar means complex conjugate. Its maxima appear at the zeros of $J_1(k_{\rho,pl}R_2)$, i.e., the zeros of Eq. (7).

If we increase the index of the cladding, this will lead to an increase of $k_{\rho,pl}$ by almost the same factor, and thus the optimal value of R_2 will decrease. And indeed, for $n_{cl} = 2$ the optimal value of R_2 is 160 nm, and the corresponding enhancement of I_S is given in Fig. 6 as a

#90072 - $15.00 USD Received 26 Nov 2007; revised 15 Jan 2008; accepted 15 Jan 2008; published 1 Feb 2008

function of R_3, together with the dependence of Eq. (7) with $k_{\rho,pl} = k_0\ (2.1423 + i\ 0.037)$. As in Fig. 5, the maximum of I_S appears close to the zero of Eq. (7).

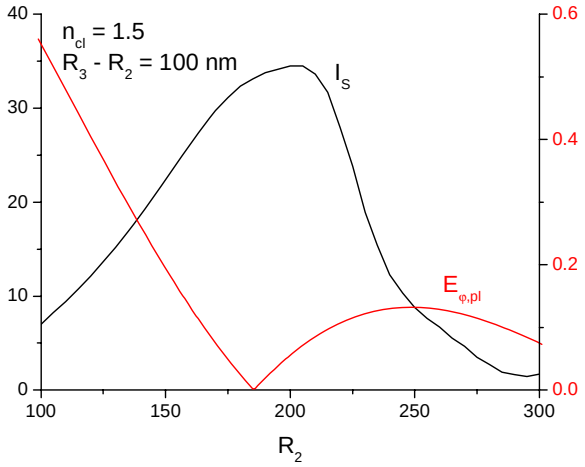

Fig. 5. Comparison of the position in R_2 of the maximum of the enhancement factor I_S with the minimum of the surface plasmon electric field components tangential to the channel wall

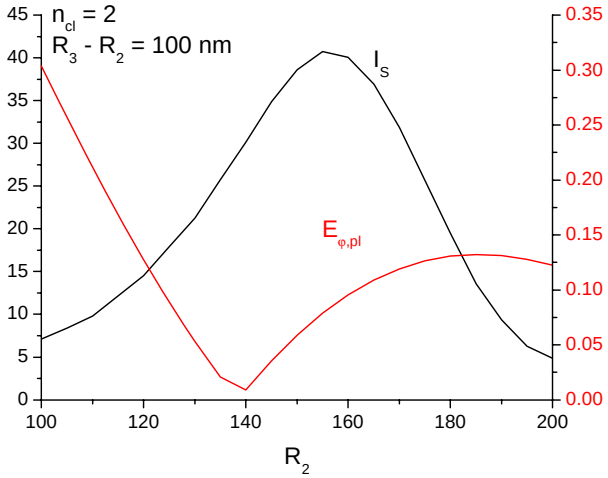

Fig. 6. Same as in Fig. 5 but for a higher cladding index $n_{cl} = 2$

4.2. The role of the channel external wall

Like the internal channel wall, the external one also serves as a perturbation that couples the incident wave into the plasmon surface wave, but the sign of this perturbation is opposite to the perturbation at R_2 [12], so that the cumulative effect of the two walls is given by applying twice Eq. (8):

#90072 - $15.00 USD Received 26 Nov 2007; revised 15 Jan 2008; accepted 15 Jan 2008; published 1 Feb 2008

$$\frac{1}{2\pi}\int_0^{2\pi}\rho\, d\varphi\, \vec{E}_{pl}.\vec{\bar{E}}_{inc}\Big|_{R_2,R_3} = R_2 J_0(k_{\rho,pl}R_2) - R_3 J_0(k_{\rho,pl}R_3) \qquad (9)$$

This result as a function of R_3 when R_2 = 200 nm is presented in Fig. 7 together with the numerical values of the amplitude of the surface plasmon electric field, both curves presenting qualitatively similar behavior.

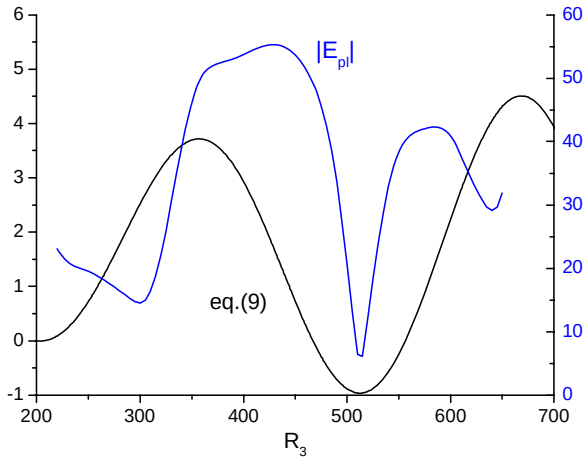

Fig. 7. Absolute value of the electric field amplitude of the plasmon surface wave (in blue) as a function of R_3 when R_2 = 200 nm and n_{cl} = 1.5, compared with the coupling between the incident light and the plasmon, as given in Eq. (9)

More detailed analysis requires taking into account the cavity modes and their coupling with the surface plasmon. The difficulty is that the model of a coaxial channel with perfectly conducting walls is not valid for quantitative analysis. On the other hand, taking into account the influence of the finite conductivity on the mode propagation constant and field distribution, together with its coupling with the surface plasmon, requires for detailed electromagnetic analysis, which is made using the numerical code based on a rigorous electromagnetic method.

A qualitative understanding of the link between the field enhancement in the central aperture and the cut-off radius of the channel groove can be found using the following argument. As it is well-known, the real part of the propagation constant $k_{\rho,pl}$ of the plasmon surface wave along the finitely but highly conducting surface is slightly higher than the free wavenumber $k_0 n_{cl}$ in the cladding, as observed from the numerical values given in the previous subsection. This leads to small but almost purely imaginary values of the wavenumber $k_{z,pl}$ along the z-axis (i.e., the surface plasmon field is evanescent in the cladding). Such values of k_z correspond to cavity modes that are just slightly below their cut-off. Thus, the surface plasmon will couple more efficiently with the cavity modes that lie close below their cut-off.

This explains the maxima of the enhancement factor I_S observed in Fig. 4 for values of R_3 lying just below the mode cut-off positions (R_3 = 325, 475, and 630 nm). The minimum around R_3 = 500 nm is already explained in connection with Fig. 7 and is due to the interaction between the incident wave and the surface plasmon. The first maximum in Fig. 4 at R_3 = 250 nm is probably due to the excitation of the mode H_{11}, but we were not able to find a simple direct link.

#90072 - $15.00 USD Received 26 Nov 2007; revised 15 Jan 2008; accepted 15 Jan 2008; published 1 Feb 2008

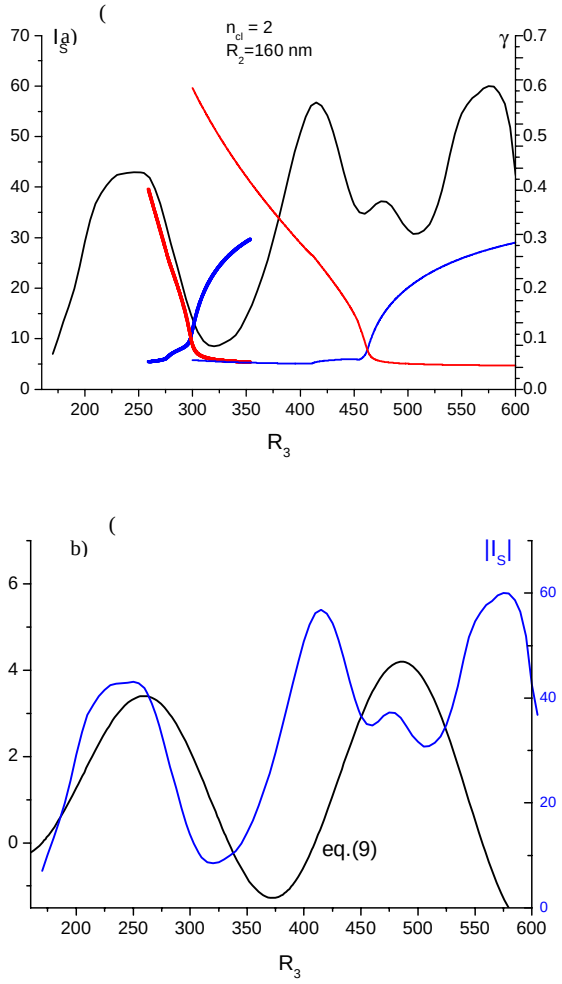

Fig. 8. Response (as in Figs. 4 and 7) as a function of R_3 of the structure with cladding index n_{cl}= 2 and R_2 = 160 nm. (a) I_S and γ, (b) incident wave – surface plasmon coupling integral according to Eq. (9).

Similar conclusions can be drawn for another configuration, where the cladding index is increased to n_{cl} = 2, which changes the plasmon propagation constant to $k_{\rho,pl} = k_0$ (2.1423 + i 0.037). As already shown at the end of Sec. 4.1 (Fig. 6), this change will decrease the optimal value of R_2 to approximately 160 nm. The dependence of the enhancement factor on the channel width is presented in Fig. 8, compared with the values of the cavity modes propagation constants [Fig. 8(a)], given in the vicinity of their cut-off radii. One observes that the enhancement factor has maxima lying below the mode cut-off radius. The minimum around 325 nm can be explained by the coupling strength between the incident wave and the surface plasmon, as given by Eq. (9) and presented in Fig. 8(b).

5. Conclusion

The simultaneous excitation of cavity modes in the central aperture and in the surrounding coaxial channel can lead to almost 50-fold increase in the electric field intensity in the central aperture, compared to the intensity of the incident field. The coupling between the two

#90072 - $15.00 USD Received 26 Nov 2007; revised 15 Jan 2008; accepted 15 Jan 2008; published 1 Feb 2008

cavities is made through the surface plasmon wave that propagates along the metal-cladding interface. The optimal conditions for maximum field enhancement require that the cavity mode inside the central aperture is below its cut-off. The coupling between the two cavities is made through the surface plasmon propagating along the upper metal-dielectric interface; as can be expected from general physics considerations, this coupling is the strongest when the field of the channel cavity mode matches the field of the plasmon surface wave, i.e, when the channel modes are below their cut-off. In addition, it is necessary to ensure maximum excitation of the surface plasmon by the incident wave. The results are useful in optimizing optogeometrical parameters of circular apertures in metallic screens leading to strong field enhancement.

Acknowledgment

This work has been funded by the grant ANR-05-PNANO-035-01 “COEXUS” of the French National Research Agency.

#90072 - $15.00 USD Received 26 Nov 2007; revised 15 Jan 2008; accepted 15 Jan 2008; published 1 Feb 2008